Intrinsic fluorescence spectroscopy in turbid media: disentangling effects of scattering and absorption

Markus G. Müller, Irene Georgakoudi, Qingguo Zhang, Jun Wu, and Michael S. Feld

The fluorescence from a turbid medium such as biologic tissue contains information about scattering and absorption, as well as the intrinsic fluorescence, i.e., the fluorescence from an optically thin sample of pure fluorophores. The interplay of scattering and absorption can result in severe distortion of the intrinsic spectral features. These distortions can be removed by use of a photon-migration-based picture and information from simultaneously acquired fluorescence and reflectance spectra. We present experimental evidence demonstrating the validity of such an approach for extracting the intrinsic fluorescence for a wide range of scatterer and absorber concentrations in tissue models, *ex vivo* and *in vivo* tissues. We show that variations in line shape and intensity in intrinsic tissue fluorescence are significantly reduced compared with the corresponding measured fluorescence.

OCIS codes: 170.5280, 170.7050, 290.4210, 300.2530, 300.1030.

1. Introduction

Elastic scattering in biologic tissue is ubiquitous, and the interplay of tissue absorbers and scatterers renders tissue optically turbid. As a result, the observed fluorescence from biologic tissue is often significantly distorted, and therefore the directly measured tissue fluorescence cannot be simply interpreted as the intrinsic fluorescence that is due to tissue biochemicals. Here intrinsic fluorescence is defined as the fluorescence that is due only to fluorophores, without the interference of absorbers and scatterers present. Such interference can severely distort the spectral features and render quantitative extraction of fluorophore concentrations impossible. In this report we present a technique, intrinsic fluorescence spectroscopy (IFS), for extracting the intrinsic fluorescence from the measured fluorescence, using information contained in the corresponding white-light diffuse reflectance spectrum. The use of IFS in tissue fluorescence studies is important because it provides direct biochemical information about the identity and the concentration of the tissue fluorophores.

Light impinging on a turbid medium undergoes multiple scattering and absorption before it exits and is collected. Such processes can be modeled by Monte Carlo simulations. However, this method is time consuming, since a large number of photon paths must be considered in order to obtain statistically significant results, and it provides only limited insight into the physical processes. Light propagation can also be described by the transport equation, but in many cases of interest it can be solved only numerically. Analytical solutions are known for special cases. In particular, the diffusion approximation accurately describes light propagation when scattering dominates over absorption. However, in the blue region of the spectrum, where tissue fluoresces strongly, absorption is often substantial, rendering the diffusion approximation less accurate. Therefore a photon migration model was used in this study.

Many researchers have used fluorescence spectroscopy for tissue diagnosis.[1–10] Biochemical changes that occur during the development of conditions such as epithelial neoplasias can alter the tissue fluorescence spectra. Unfortunately, tissue absorption changes (in hemoglobin, melanin, water, and the like) can also alter the measured fluorescence spectra. Some studies have taken this into account. Anidjar *et al.*[6] were able to distinguish between normal and cancerous bladder tissue by exciting the tissue with 308-nm light and taking the intensity ratio of the

The authors are with the Laser Biomedical Research Center, George R. Harrison Spectroscopy Laboratory, Massachusetts Institute of Technology, Cambridge, Massachusetts 02139. M. S. Feld's e-mail address is msfeld@mit.edu.

Received 9 January 2001; revised manuscript received 23 April 2001.

0003-6935/01/254633-14$15.00/0

measured fluorescence at two wavelengths of the emission spectrum, 360 and 440 nm. Since the hemoglobin absorption is similar at these two wavelengths, the fluorescence ratio (diagnostic index) is largely independent of hemoglobin, the dominant absorber at these wavelengths. A similar technique was also employed by Liu *et al.*,[2] who used the ratio of fluorescence intensities at 340 and 440 nm, excited at 300 nm, to distinguish cancerous from normal breast tissue. One disadvantage of these algorithms is that only two wavelengths of a spectrum are used. With intrinsic fluorescence, it should be possible to use the entire spectrum for tissue classification and, in addition, to obtain quantitative information about the contributing tissue fluorophores (biochemical composition).

The recovery of intrinsic fluorescence is also of interest in cases in which the selective accumulation of an exogenously administered fluorophore such as Photofrin, meso-tetrahydroxyphenylchlorin, or 5-aminolevulinic acid (5-ALA) induced protoporphyrin IX (PpIX) is used to detect or treat cancerous or precancerous lesions.[11,12] However, the measured fluorescence intensity associated with such drugs or their endogenously induced fluorophores is dependent on the local absorber (e.g., hemoglobin) concentration, which can alter the measured fluorescence intensity. Here, too, the intrinsic fluorescence could provide more-reliable information about the drug concentration in tissue,[13,14] which could in turn be used for disease diagnosis or for monitoring dosimetry during photodynamic therapy of cancer. The fluorescence intensity of the photosensitive dye in photodynamic therapy varies with concentration and oxygen saturation of hemoglobin, and it is difficult to estimate the actual dye concentration and its photobleaching.[15,16]

Recovery of the intrinsic tissue fluorescence allows one to isolate changes in the tissue fluorophores from changes in other tissue optical properties, such as hemoglobin or beta-carotene absorption. Indeed, studies of diffuse reflectance[17–19] and frequency-domain photon migration[20] suggest that the scattering and absorption properties of cancerous lesions are different from those of normal tissues. Therefore determination of the intrinsic tissue fluorescence and analysis of tissue reflectance, in combination, would provide a more complete understanding of the biochemical and/or morphological changes that take place during the progression of disease.

The importance of extracting intrinsic fluorescence from biologic tissues, and the connection of fluorescence distortions and diffuse reflectance, has been proposed by several investigators and was initially presented by Jöbsis *et al.*[21] and by Mayevsky and Chance.[22,23] Research in this field was reviewed extensively by Ince *et al.*[24] There have been several attempts to extract the intrinsic fluorescence of turbid media from information contained in the bulk fluorescence and diffuse reflectance. Wu *et al.*[25] introduced a photon migration model based on Monte Carlo simulations, which related the measured fluorescence to the reflectance. Durkin *et al.*[26] used Kubelka–Munk absorption and scattering coefficients, obtained from diffuse reflectance and transmittance experiments, to predict the intrinsic fluorescence spectrum. Zhadin and Alfano[27] derived a formula from a simplified one-dimensional diffusion approximation. They expressed reflectance and measured fluorescence in terms of the medium's darkness, a variable defined as the ratio of the absorption coefficient to the reduced scattering coefficient. Inversion of the reflectance yielded the darkness parameter, which was then used to extract the intrinsic fluorescence line shape from the measured fluorescence. Gardner *et al.*[28] related propagation of laser excitation light and measured fluorescence to the diffuse reflectance with the help of Monte Carlo simulations. With these empirically obtained expressions, an expression for the intrinsic fluorescence was derived.

Most of these studies have been limited to the wavelength ranges of 500–700 nm (Refs. 25, 27, and 28) and 600–800 nm (Ref. 29), where hemoglobin and water absorption are not strong. However, a large number of fluorescence studies have been conducted in the 400-nm emission range,[1,4,5,7,8,30] where hemoglobin absorption is prominent and can lead to significant spectral distortions and misinterpretation of the measured fluorescence. Human tissue fluoresces very strongly in this range when excited by UV-A light and can be distorted substantially by the interplay of scattering and absorption, particularly by hemoglobin, which absorbs most strongly at ~420 nm. This absorption can give rise to a dip in the measured bulk fluorescence that can be misinterpreted, since the spectra are no longer simply a linear sum of spectral contributions from endogenous fluorophores such as collagen, NADH [nicotinamide adenine dinucleotide (NAD) with the addition of high-energy hydrogen (H)], elastin, and so on. Therefore, it is important to extract the undistorted tissue intrinsic fluorescence over a wide emission range that includes this important diagnostic region.

In this report we present experimental evidence demonstrating the validity of a method for correcting the distortions introduced in tissue fluorescence by scattering and absorption, even when the absorption coefficient, μ_a, and reduced scattering coefficient, μ_s', are of the same order. The method is based on a picture of photon migration in a turbid medium, and it expresses the intrinsic fluorescence in terms of experimentally measured fluorescence and reflectance, without the use of numerical computations.[31] Several steps were used to explore the validity of this method in the 370–700-nm emission range. First, we used a physical tissue model (phantom), consisting of scattering spheres of known diameter and refractive index and mixtures of chemicals with known absorption and fluorescent properties, suspended or dissolved in water. The well-controlled optical parameters of these turbid tissue models could be varied to fully span the range of biologic tissues. We then studied minced (homogenized) samples of hu-

man oral tissue; this provided a uniform, homogenous medium with known intrinsic fluorescence. In addition, we examined intact *in vitro* tissue samples, as well as *in vivo* tissue fluorescence and diffuse reflectance taken during clinical procedures. We found that the modeled intrinsic fluorescence extracted with the photon migration method is in excellent agreement with the actual intrinsic fluorescence of the tissue models in terms of both line shape and intensity. Finally, we analyzed the spectral composition of the intrinsic tissue fluorescence by comparing it with fluorescence spectra of pure biochemicals.

2. Photon Migration Theory

To extract intrinsic fluorescence from experimentally measured tissue fluorescence and reflectance, Zhang *et al.*[31] extended and refined a method based on the photon migration picture introduced by Wu *et al.*[25] In this picture, light propagation in a turbid medium is described in terms of photons traveling in paths with discrete photon–tissue interaction events (nodes) of absorption, scattering, and fluorescence. The light is delivered and collected by an optical fiber probe or other source–detector system of fixed geometry. Two elementary properties are associated with each photon path: the escape probability, ρ, and the photon weight, w. For the case of diffuse reflectance, ρ denotes the escape probability of a photon that enters the medium, undergoes n scattering events, and is collected after exiting, and w_n denotes the corresponding weight (survival fraction) of the injected photon. For fluorescence, ρ and w have indices (n, i), denoting i scattering events at the excitation wavelength, λ_x, followed by fluorescence at the $(i + 1)$th event and then followed by $n - i - 1$ scattering events at the fluorescence emission wavelength, λ_m (see Appendix A for list of symbols). In this picture we assume that the phase-function dependence of the scattering can be separated from the scattering and absorption coefficients.[25] The diffuse reflectance, R, and the measured fluorescence, F, can then be expressed as

$$R(\lambda) = \sum_{n=1}^{\infty} \rho_n w_n, \tag{1a}$$

$$F_{xm} \equiv F(\lambda_x, \lambda_m) = \sum_{n=1}^{\infty} \sum_{i=0}^{n-1} \rho_{ni} w_{ni}, \tag{1b}$$

where

$$w_n = a^n, \tag{1c}$$

$$w_{ni} = a_x^{i+1} \frac{f_{xm}}{\mu_{sx} l} a_m^{n-i-1}, \tag{1d}$$

$$f_{xm} = (I_x / h\nu_x) \mu_{fx} l \phi_{xm} h\nu_m, \tag{1e}$$

where the subscripts x and m indicate the dependence of the quantity on excitation and fluorescence emission wavelengths, respectively. The albedo, a, is defined as $a = \mu_s/(\mu_a + \mu_s)$, where μ_a and μ_s denote the absorption and the scattering coefficient of the medium, respectively. The quantity l is a constant with dimension of length that characterizes a given light delivery–collection scheme and can be related to the effective depth from which fluorescence is collected by the probe. The fluorescence quantum yield is denoted by ϕ_{xm}. The intrinsic fluorescence and the absorption coefficient of the fluorophore are denoted by $f_{xm} = f(\lambda_x, \lambda_x)$ and μ_{fx}, respectively.

On the basis of Monte Carlo simulations and experiments,[25,31] we approximate the escape probability to calculate R and F as

$$\rho_n = \alpha \exp(-\beta n), \tag{2a}$$

$$\rho_{ni} = (\alpha_x \alpha_m)^{1/2} \exp[-\beta_x (i + 1)] \exp[-\beta_m (n - i - 1)]. \tag{2b}$$

Here $\beta = S(1 - g)$, with S a constant that depends on the specific light delivery–collection geometry of the probe, and g is the anisotropy parameter of the medium.[25] Note that μ_a, μ_s, and g are all wavelength dependent. Equation (2b) takes into account the wavelength change from excitation to emission, and, in the limit in which the excitation wavelength approaches the emission wavelength, Eq. (2b) reduces to Eq. (2a), as it must. The quantity α can be related to R_0, the diffuse reflectance in the absence of absorption ($\mu_a = 0$, $a = w_n = 1$): $R_0 = \sum_{n=1}^{\infty} \rho_n = \alpha/\epsilon$, with $\epsilon = \exp(\beta) - 1$.

When we insert Eqs. (2) into Eqs. (1a) and (1b), F and R can be evaluated exactly and combined to provide an expression for the intrinsic fluorescence[31]:

$$f_{xm} = \frac{F_{xm}}{\dfrac{1}{\mu_{sx} l} \left(\dfrac{R_{0x} R_{0m}}{\epsilon_x \epsilon_m} \right)^{1/2} \dfrac{R_x}{R_{0x}} \left(\dfrac{R_m}{R_{0m}} + \epsilon_m \right)}. \tag{3}$$

Equation (3) is the basis of the IFS method, providing a relationship that enables the intrinsic fluorescence spectrum to be extracted from the measured fluorescence, by use of the diffuse reflectance collected from a given tissue site with the same probe. This is possible because absorption and scattering distort the measured fluorescence and reflectance similarly, since diffusely reflected and fluorescence photons delivered and collected by the same probe traverse similar paths. Also, note that F and f are functions of both excitation and emission wavelengths so that the full intrinsic fluorescence excitation–emission matrix (EEM), f_{xm}, can be obtained from the measured fluorescence EEM, F_{xm}. The method presented above employs the framework of the photon migration picture of Ref. 25, but the form of the fluorescence escape probability has been modified [Eq. (2b)]. This modification allows us to evaluate the intrinsic fluorescence without further assumptions. The sums describing F and R can be evaluated exactly, instead of being approximated by integrals. This integral approximation limited the applicability of the previ-

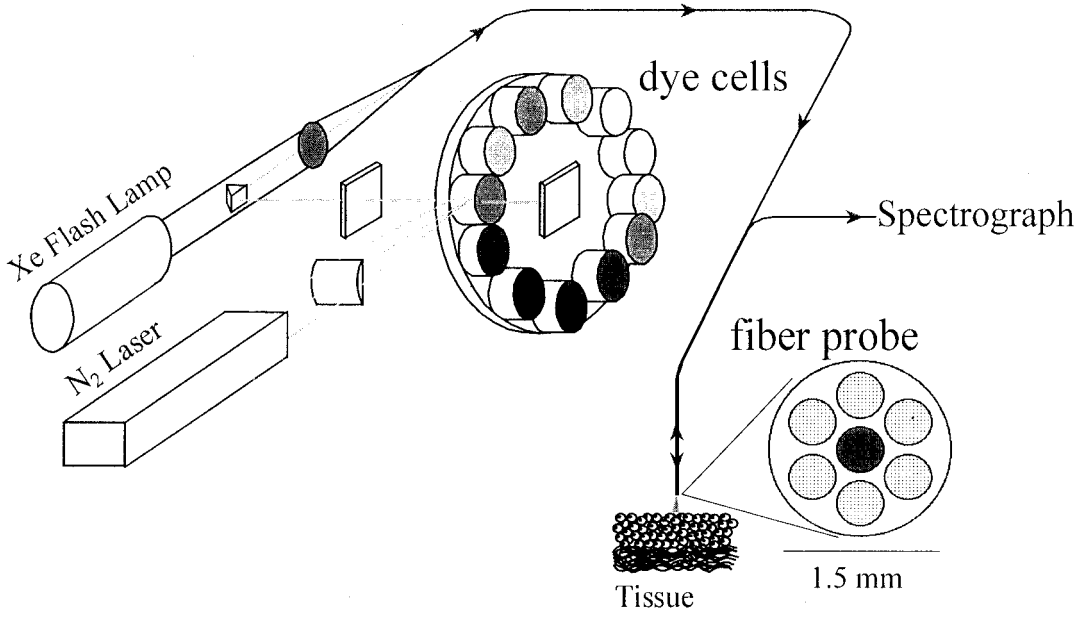

Fig. 1. FastEEM instrument. Flash-lamp source is used for reflectance spectroscopy, (dye) laser source for fluorescence spectroscopy. The nitrogen laser pumps the dye cells to obtain ten dye laser wavelengths. A fiber-optic probe is used for light delivery and collection.

ous method to values of the albedo approaching 1.[32] Below, we validate Eq. (3) on physical tissue models with completely specified optical properties, and then we show how it can be employed to analyze biologic tissues, when the optical properties are not known *a priori*. Note that ϵ is always smaller than R/R_0, which in turn is less than 1 (see Section 5).

It is interesting to consider two limiting cases:

$R/R_0 \gg \epsilon$. This is the case for which absorption is so weak that R/R_0 is relatively large compared with ϵ. (Note that $R/R_0 \leq 1$). Then Eq. (3) reduces approximately to $f_{xm} \propto F_{xm}/R_m$, with the proportionality constant being nearly independent of λ_m. Thus this limit provides a simple procedure for extracting the intrinsic fluorescence line shape.

$R/R_0 = 1$: In this case there is no absorption, and Eq. (3) reduces to

$$f_{xm} = \frac{F_{xm}}{\frac{1}{\mu_{sx} l}\left(\frac{R_{0x}R_{0m}}{\epsilon_x \epsilon_m}\right)^{1/2}(1 + \epsilon_m)}. \quad (4)$$

This expression indicates that scattering has little influence on the measured fluorescence line shape, since the denominator is weakly dependent on emission wavelength. However, scattering has a substantial effect on the overall fluorescence intensity.

3. Materials and Methods

To explore the accuracy of the above model, we conducted a series of reflectance and fluorescence spectroscopic studies (Section 4), using physical tissue models with optical properties similar to those of biologic tissue and using minced human oral tissue. A brief description of the instrumentation and materials used in these studies follows.

A. Instrumentation

All reflectance and fluorescence spectra were obtained with a FastEEM instrument (Fig. 1).[33] A xenon flash lamp (EG&G Optoelectronics, FX-139, Salem, Massachusetts) was used as a white-light source to acquire reflectance spectra in the 360–700-nm range. Excitation light sources for fluorescence measurements were provided by a 337-nm-wavelength nitrogen laser (Laser Science, Inc., Franklin, Massachusetts) and ten different dye lasers (358–610 nm), sequentially pumped by the nitrogen laser. The dye cuvettes were mounted on a rotating wheel driven by a stepper motor. Light was delivered to the tissue and collected by means of a probe[34] containing seven optical fibers (200-μm core diameter), one fiber used for light delivery and six for collection. At the distal tip the collection fibers surrounded the delivery fiber and were fused together, creating a quartz shield approximately 1.5 mm in diameter, which was beveled and then polished at a 17° angle to reduce internal reflections at the boundary between glass and tissue. During a measurement, the probe tip was brought into contact with the sample under investigation, thus providing a fixed light delivery–collection geometry. Data were taken either in an open field or through the biopsy channel of an endoscope. Fluorescence and reflectance were collected by the collection fibers through the same probe tip. A wheel of long-pass filters was used to prevent reflected laser excitation light from reaching the spectrograph (CP 200, Jobin Yvon SA, Edison, New Jersey) and the intensified diode array detector (EG&G Princeton Applied Research, Trenton, New Jersey). Fluorescence spectra at 11 excitation wavelengths and a reflectance spectrum were collected in less than 5 s. The whole system was

controlled by a 486× personal computer, and spectra were recorded with Oma Vision (EG&G Princeton Applied Research, Trenton, New Jersey) software. The wavelength scale was calibrated with a mercury lamp. A concentrated barium sulfate suspension (concentration, >20%) was used for reflectance calibration.

B. Physical Tissue Models

The physical tissue models were suspensions of polystyrene microspheres (1-μm diameter, Polybead, Polyscience, Warrington, Pennsylvania), a water-soluble dye (Furan 2 Lambdachrome, Fort Lauderdale, Florida), and ferrous human hemoglobin powder (Sigma Chemicals, St. Louis, Missouri) dissolved in deionized water. Hemoglobin is the major absorber in the visible wavelengths for tissues of interest,[19] and Furan 2 fluoresces in the same range as collagen under UV-A excitation. Polystyrene beads were used to simulate the scattering and anisotropy coefficients of tissue,[19,35] which were calculated by use of Mie theory.

The components of the physical tissue model were mixed in a glass bottle and diluted with deionized water to the concentration of interest. The optical fiber probe was immersed in the medium to obtain an easily reproducible geometry. The inside diameter of the bottle was 1.3 cm, which is ~35 times larger than the transport mean free path at wavelengths of interest. Thus, edge effects were insignificant. Experiments performed on models in larger bottles with different boundaries showed no differences in fluorescence and reflectance spectra. For the physical tissue model experiments, only excitation at 337 and 358 nm resulted in appreciable fluorescence, since the extinction coefficient of the dye (Furan 2) is negligible beyond 370 nm.[36]

To correct for background fluorescence, fluorescence spectra from water suspensions containing only polystyrene beads at a given concentration were subtracted from the samples containing dye at the same polystyrene bead concentration. This background signal was small, less than 5% of the Furan fluorescence signal, and proportional to the polystyrene bead concentration. Its removal ensured that the analyzed fluorescence in these spectra was due to the fluorophore only.

C. Minced Human Tissue Models

To determine the applicability of the theory to biologic tissue, we acquired fluorescence EEMs and reflectance spectra from normal samples of cadaver oral cavity tissue. Since the penetration of visible light in tissue is of the order of 1–2 mm, it was not necessary to consider contributions to the measured fluorescence that are due to tissue beneath the submucosa. Thus, tissue sections containing only epithelium and submucosa were separated from the rest of the bulk tissue specimen, frozen with liquid nitrogen, and then minced in a mortar with a pestle to create a homogeneous distribution of a mixture of endogenous tissue chromophores. After thawing, the tissue resembled a thick gel. By adding more hemoglobin, we were able to vary the absorption properties of the tissue mince. Significant autofluorescence signals were observed from 380 to 700 nm for excitation wavelengths from 337 to 500 nm. Thus, studies with minced tissue provided a homogenous and reproducible medium with a uniform distribution of fluorophores, which allowed us to test the theory for a wide range of excitation and emission wavelengths. The intrinsic fluorescence of minced tissue was obtained experimentally from a very thin layer (~10 μm) placed on a microscope slide. Since the absorption and scattering mean free paths in tissue are longer than 10 μm, scattering and absorption do not alter the fluorescence of a thin section.

D. *In vivo* and *in vitro* Tissue Experiments

We also recorded bulk autofluorescence of intact oral cavity tissue to determine the effect of the layered structure of tissue on the measured autofluorescence by placing the fiber probe tip on the tissue surface. Additionally, we obtained *in vivo* fluorescence of normal oral cavity tissue to assess changes caused by tissue extraction and processing. We also obtained *in vivo* spectra of squamous esophageal tissue from patients undergoing routine endoscopy. In this case, the probe was passed through the biopsy channel of the endoscope and brought into gentle contact with the tissue. Finally, we compared fluorescence spectra of pure collagen, elastin, and NADH (Sigma Chemicals, St. Louis, Missouri), extracted biochemically, with the obtained intrinsic tissue fluorescence spectra.

4. Results

A. Effects of Scattering

To investigate how scattering affects the intensity and the spectral shape of a fluorescence spectrum, fluorescence spectra were acquired for a series of physical tissue models with different scattering coefficients and negligible absorption. The models contained deionized water, Furan 2 (0.7 μM), and 1-μm diameter polystyrene beads at concentrations between 0 and 4×10^{10} beads/ml (0–2% volume concentration), corresponding to variations in the reduced scattering coefficient, μ_s', from 0 to 10 mm^{-1} in the visible spectral range (the anisotropy, g, was approximately 0.85–0.93 in the UV–visible range). Spectra at 13 different μ_s' values were obtained with 337- and 358-nm excitation. Representative spectra excited at 337 nm are shown in Fig. 2(a). The corresponding white-light diffuse reflectance spectra are presented in Fig. 2(b). Fluorescence spectra of a dilute aqueous solution of Furan 2 (0.7 μM) were recorded at 337- and 358-nm excitation wavelengths. The acquired fluorescence emission spectrum excited at 337 nm, denoted by i in Fig. 2(a), provided the measured intrinsic fluorescence for the physical tissue models discussed in the Subsections 4.A.1 and 4.B.

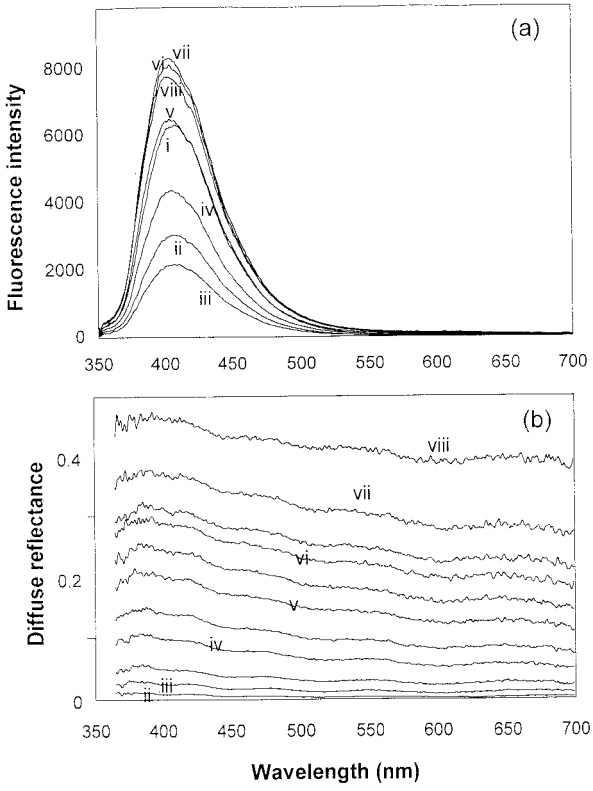

Fig. 2. (a) Fluorescence emission spectra (337-nm excitation) and (b) corresponding reflectance spectra of physical tissue models. Curve i, for a dilute dye solution, gives the intrinsic fluorescence. In curves ii–viii the concentration of polystyrene beads is progressively increased. In volume percent, (i) 0, (ii) 0.016, (iii) 0.065, (iv) 0.325, (v) 0.65, (vi) 0.975, (vii) 1.3, (viii) 1.95. This provided values of μ_s' ranging from 0 to 10 mm^{-1} at $\lambda = 400$ nm. Note that in these studies $\mu_a = 0$. Fluorescence intensity is in detector counts. The collected reflectance is in units of fraction of incident light.

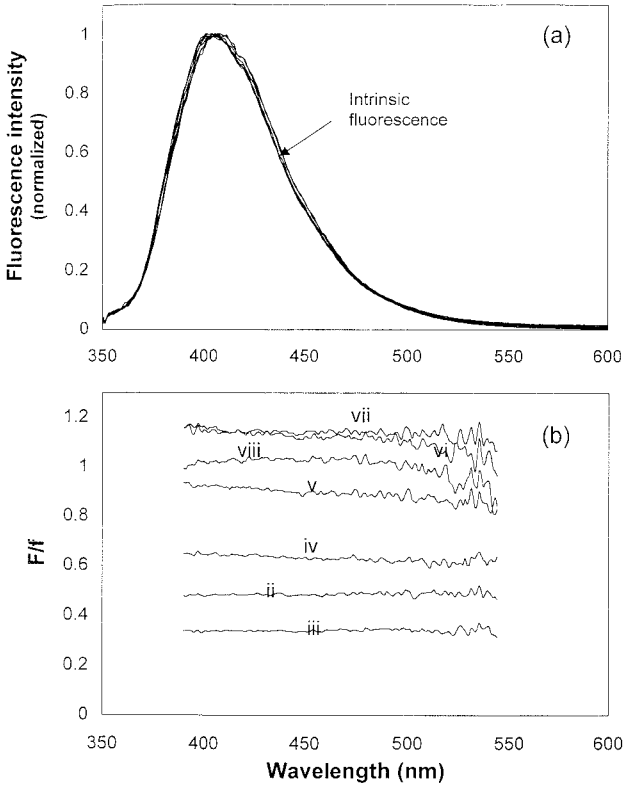

Fig. 3. (a) Fluorescence emission spectra of Fig. 2(a), normalized to their peak heights; (b) fluorescence ratio spectra, obtained from the curves of Fig. 2(a) by division by the intrinsic fluorescence, curve i. Note the small line-shape differences between the intrinsic fluorescence and the fluorescence with scatterers present.

1. *Spectral Shape*

The normalized fluorescence emission spectra of Fig. 2(a) were all similar to the intrinsic fluorescence line shape of the pure Furan dye [Fig. 3(a)] However, the ratio of the observed fluorescence spectra to the intrinsic fluorescence, F/f, revealed small changes in line shape of approximately 5% over 150 nm [Fig. 3(b)]. This is consistent with Eq. (4) and Monte Carlo simulations of fluorescence from a highly scattering medium with very small absorption ($\mu_a \approx 0.01\ \mu_s'$), collected by a finite-size probe with a collection angle of 12° (N.A. = 0.22; Fig. 4). However, the spectral line shapes of the corresponding diffuse reflectance spectra varied in intensity by as much as 15% over 150 nm [Fig. 2(b)]. As discussed in Section 5, these more substantial line shape variations are expected, since reflected light experiences the effects of scattering over its entire path in the medium, whereas fluorescence emission is generated in the medium and subjected to scattering over a path roughly half the length of the diffuse reflectance path.

2. *Concentration Dependence*

In contrast to the small effect of scattering on the fluorescence line shape, the fluorescence intensity varied appreciably with scatterer concentration (Fig. 5). At the smallest values of scatterer concentrations, where the mean free path is relatively large, the fluorescence intensity decreased nearly exponentially with increased scatterer concentration. For

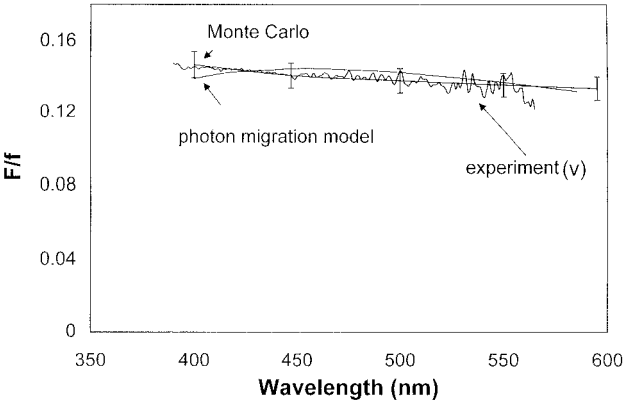

Fig. 4. Fluorescence ratio spectra: prediction [Eq. (4)], Monte Carlo simulation and experiment [curve v from Fig. 3(b)]. Error bars (5%) are due to fluctuations in Monte Carlo simulations because of finite numbers of photons.

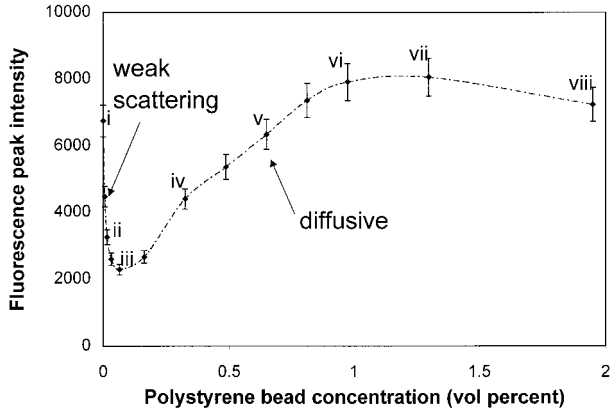

Fig. 5. Peak fluorescence intensity of physical tissue models as a function of polystyrene bead concentration. The peak values are taken from the spectra of Fig. 2(a). The error bars indicate the laser shot-to-shot excitation variations and accuracy of dye concentrations.

larger values of μ_s' photons undergo increased scattering, and the light becomes diffuse. In this regime (polystyrene bead concentration >0.065 in volume percent, transport mean free path $1/\mu_s' < 4$ mm), the fluorescence intensity increased with scatterer concentration. At the highest concentrations the fluorescence intensity plateaued.

B. Effects of Combined Scattering and Absorption

To understand the manner in which absorption affects fluorescence in the presence of scattering, we conducted a second set of fluorescence and reflectance measurements. In these experiments the physical tissue models contained fixed concentrations of Furan 2 (0.9 μM) and polystyrene beads (0.65% in volume, with $\mu_s' \approx 2$ mm^{-1}), and varying amounts of hemoglobin. The concentration of hemoglobin, mainly present in its oxygenated form, was varied from 0 to 2 g/l (up to 30 μM, corresponding to $\mu_a = 4$ mm^{-1} at 420 nm), which is the relevant range for most human tissues.[19,20]

Figure 6(a) presents fluorescence spectra for ten different hemoglobin concentrations. With increasing hemoglobin concentration, the fluorescence intensity decreased, and the fluorescence line shape was altered significantly. To illustrate more clearly the substantial absorption effects that occur with increasing hemoglobin concentration, we show in Fig. 6(b) normalized fluorescence spectra of an optically thin sample (intrinsic fluorescence) and a turbid sample with 1.5 g/l hemoglobin concentration. The characteristic oxyhemoglobin absorption features are clearly visible in the fluorescence [Figs. 6(a) and 6(b) and in the corresponding reflectance spectra [Fig. 6(c)]. The oxyhemoglobin absorption peaks produce dips at approximately 415, 540, and 580 nm in the reflectance spectra and at 415 nm in the fluorescence spectra.

To use the model to extract intrinsic fluorescence in the presence of hemoglobin absorption, a number of

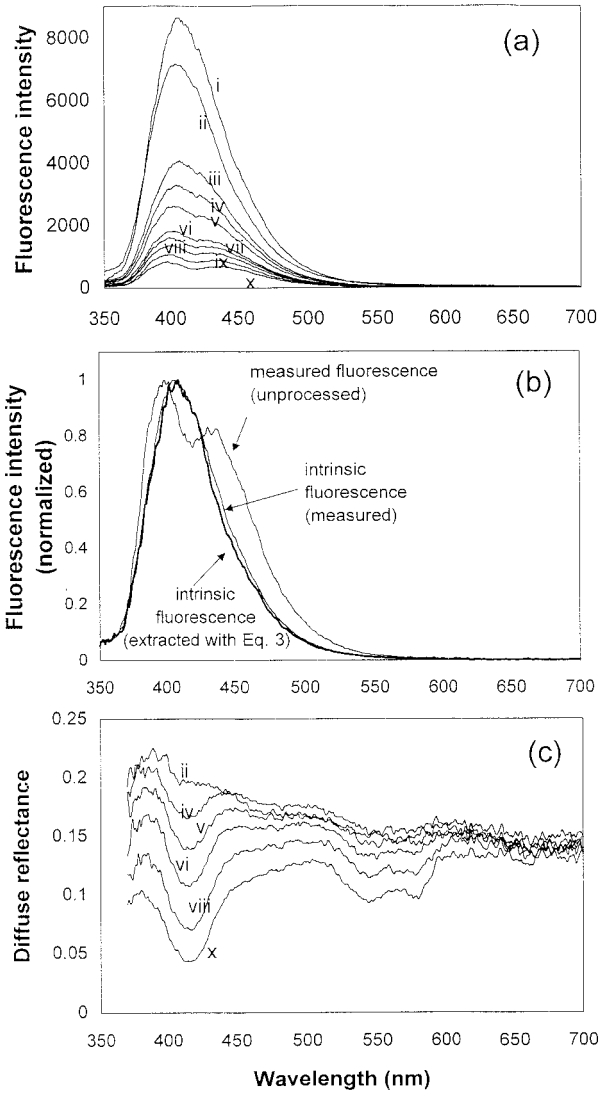

Fig. 6. Effects of absorption and scattering on observed fluorescence. (a) Fluorescence spectrum of a dilute solution of dye (i) (intrinsic fluorescence) and physical tissue models with a fixed scatterer concentration and different concentrations of hemoglobin added: (ii) 0, (iii) 0.05, (iv) 0.125, (v) 0.25, (vi) 0.5, (vii) 0.75, (viii) 1, (ix) 1.5, (x) 2 g/l; (b) comparison of measured and extracted intrinsic fluorescence and observed fluorescence of a sample [Fig. 6(a), ix] with hemoglobin (1.5 g/l). All spectra are normalized. (c) Reflectance spectra of physical tissue models with various absorber concentrations. Note that the intensity decreases in (a) and (c) with increasing hemoglobin, especially at the major oxyhemoglobin absorption peak (415 nm). In all the above data, μ_s' was held constant at approximately 2 mm^{-1}.

parameters had to be determined. The only significant contribution to the absorption coefficient, μ_a, of the physical tissue models was due to hemoglobin, since light absorption by Furan, polystyrene beads, and water is negligible. With knowledge of the hemoglobin concentrations, one can readily evaluate the absorption coefficient from the measured extinction coefficients for oxyhemoglobin and deoxyhemoglobin.[37] For the range of hemoglobin concentrations used, the peak absorption coefficient (at 415 nm) was

smaller or of the same order as the reduced scattering coefficient, which typically varies between 1 and 3 mm^{-1} in human tissues. Since the hemoglobin solution was used under ambient conditions (partial oxygen pressure, 154-mm mercury, and room temperature) at pH 7, the hemoglobin was mostly in its oxygenated form. The scattering cross section, $\sigma_s(\lambda)$, and the anisotropy parameter, $g(\lambda)$, of the polystyrene beads were calculated from Mie scattering theory[38] by use of the known diameter and refractive index of the beads and water. From these values we calculated the reduced scattering coefficient $\mu_s' = \mu_s(1 - g)$, where $\mu_s = n_s\sigma_s$, with n_s the polystyrene bead density (in the experiments, $n_s = 1.25 \times 10^7\ mm^{-3}$, $\mu_s' \approx 2\ mm^{-1}$ at 550 nm). The parameter ϵ, defined in Section 2, was dependent only on g and the probe-specific parameter S of Eq. (3). Since different values of S affect the line shape differently, the best value of S was determined by means of fitting a modeled intrinsic fluorescence spectrum with known optical properties to the measured intrinsic fluorescence spectrum, with Eq. (3). Using this procedure, we found S to be close to 1 for our system, and this value was used for the analysis of subsequent experiments. Because the xenon flash-lamp intensity was weak at 337 and at 356 nm, the diffuse reflectance values at these excitation wavelengths with and without absorption, R_x and R_{0x}, respectively, were obtained by use of a diffuse reflectance model appropriate for our experimental setup.[19,39] The optical parameters μ_s' and μ_a obtained by means of fitting this model to the data were in good agreement with those calculated with the known concentrations of hemoglobin and polystyrene beads (μ_s' was calculated with Mie theory). Thus, in the case of tissue model experiments, both methods could be used to calculate the unknown parameters. All other variables, F_{xm}, R_m, and R_{0m}, were acquired experimentally.

Having obtained the values of the model parameters and the experimentally measured fluorescence and reflectance spectra, we used our photon migration model, Eq. (3), to extract the intrinsic fluorescence. The distortions in the measured fluorescence spectra introduced by absorption and scattering were eliminated in the modeled intrinsic fluorescence line shape [Fig. 7(a)]. Good agreement between the modeled and the measured intrinsic fluorescence line shape was obtained for all hemoglobin concentrations [Fig. 7(a)]. In addition to obtaining the correct intrinsic fluorescence line shape, we also recovered the fluorescence intensity information up to a constant scaling parameter l with an accuracy greater than 90% [Fig. 7(b)]. The value for l, approximately 220 μm for the probe used, was obtained by means of comparing the modeled intrinsic fluorescence intensity with the experimentally measured fluorescence of a dilute dye solution of the same fluorophore concentration at 337- and 358-nm excitation.

Experiments with fixed hemoglobin content and varying bead concentrations (0.3–0.8% in volume)

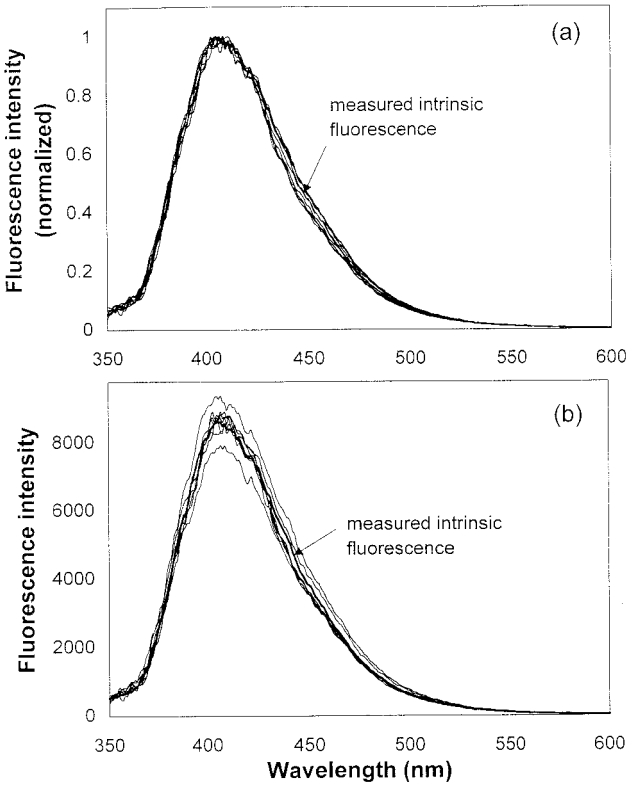

Fig. 7. Intrinsic fluorescence emission spectra, extracted from turbid physical tissue models Fig. 6(a), $\lambda_x = 337$ nm: (a) normalized, (b) unnormalized. The measured intrinsic fluorescence is indicated. Note in (a) the excellent agreement of the corrected line shapes. The intensity differences in (b) are small, indicating good intensity corrections of data varying in intensity by an order of magnitude [compare Fig. 6(a)]. Analysis of the data gives l = 220 μm. See text for details.

resulted in equally good agreement between the modeled and the measured intrinsic fluorescence.

In summary, the intrinsic fluorescence of the Furan 2 dye was obtained at two excitation wavelengths: 337 and 358 nm. The double peak observed in the measured fluorescence (337-nm excitation) in the 400-nm region became a single peak in the extracted intrinsic fluorescence. The decreased peak intensity observed in the measured fluorescence with increasing hemoglobin concentration was also corrected, and the same intrinsic fluorescence line shape and intensity were recovered for samples with the same fluorophore content but varying hemoglobin concentrations. Thus the model was found to recover successfully the intrinsic fluorescence of turbid media over a wide range of physiologically relevant absorption and scattering coefficients.

C. Minced Tissue Studies

To determine whether our model can recover the intrinsic fluorescence of samples that have the actual scatterers, absorbers, and fluorophores of biologic tissue, we collected diffuse reflectance and EEM fluorescence from minced oral cavity tissue. In contrast to the experiments with physical tissue models, spec-

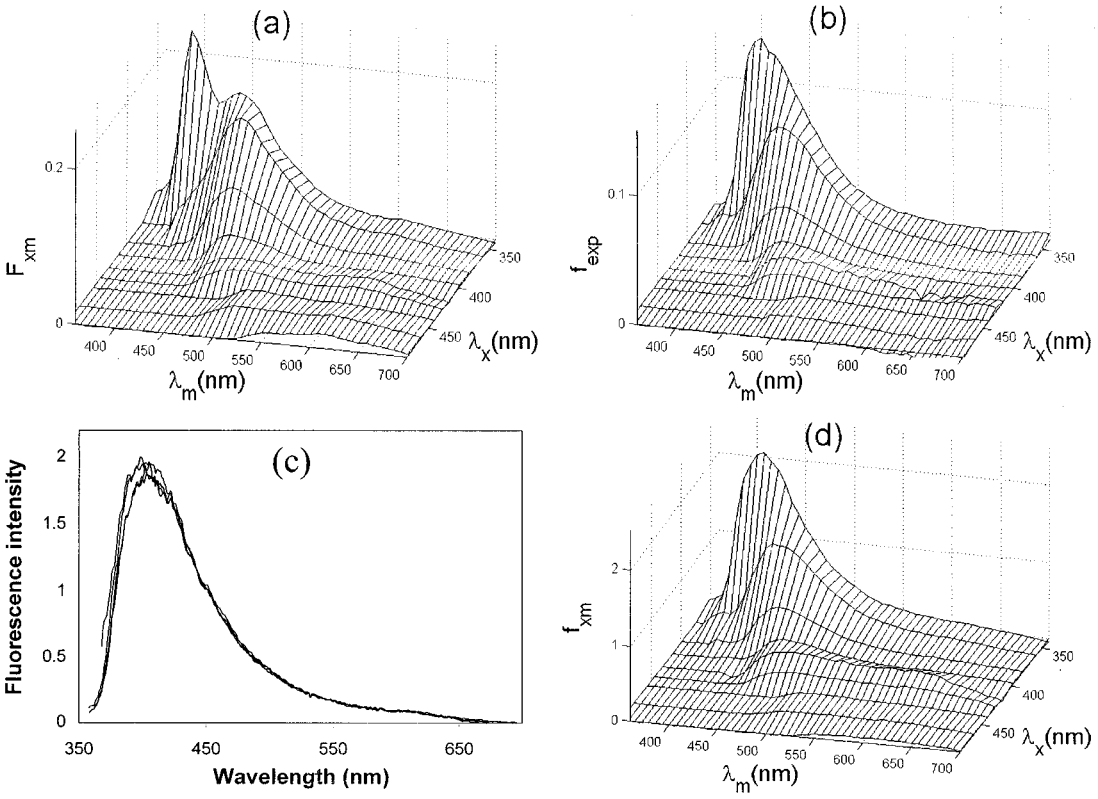

Fig. 8. EEMs of minced oral cavity tissue. (a) Minced tissue (~2 g/l Hb concentration and 4-mm thickness). (b) Intrinsic fluorescence EEM of a thin section of minced tissue (~10-μm thickness); absorption and scattering effects are negligible. (c) Extracted intrinsic fluorescence for minces with hemoglobin concentrations ranging from 0.7 to 4.7 g/l, λ_x = 337 nm. (d) Extracted intrinsic fluorescence EEM of minced tissue. The similarity between (b) and (d) and the dissimilarity between (a) and (b,d) show the usefulness of the intrinsic fluorescence extraction method. Note that the hemoglobin dip in (a) has vanished. The 20-fold intensity difference between (b) and (d) corresponds well to the difference in the thickness of the thin section (~10 μm) and the fluorescence collection depth (l = 220-μm probe parameter). The tenfold intensity difference between (a) and (d) is reasonable [compare Fig. 6(a)].

tral features over a wide range of wavelengths (370–700 nm) were observed both in diffuse reflectance and in fluorescence excited over a variety of wavelengths (337–500 nm). This is because tissue is composed of a mixture of chromophores spanning a wide absorption and emission range. In intact tissue, hemoglobin concentration can vary greatly with tissue site as a result of factors such as inflammation. To simulate this, additional hemoglobin was added to the homogenized tissue. Measured fluorescence spectra of four minced tissue samples with varying amounts of hemoglobin were obtained, and a decrease in fluorescence intensity and distortion of the line shape was observed with increasing absorber concentration. Unlike the case of the physical tissue models, the absorption coefficient, reduced scattering coefficient, and anisotropy parameter were not available *a priori* for calculating the intrinsic fluorescence spectra. We used the model of Zonios *et al.*[19] to extract the hemoglobin concentration and the average scatterer size and density from the diffuse reflectance over the range of 360 to 700 nm. The extracted values for μ_s' ranged from 1 to 3 mm^{-1}, and the hemoglobin concentration varied between 0.7 and 4.7 g/l. The model of Zonios *et al.*[19] was then used to calculate R_x at 337 and 358 nm, and R_{0m} and R_{0x} (for $\mu_a = 0$), since in tissue it is not feasible to determine these parameters experimentally. The values of the probe-specific parameters S and l, determined previously with the physical tissue models, were used. Thus all quantities in Eq. (3) were known, and the line shape and intensity of the extracted intrinsic fluorescence of the minced tissue samples could be compared with those of the measured intrinsic fluorescence, obtained from an optically thin sample of minced tissue [Fig. 8(b)]. Good agreement was obtained in all cases. Furthermore, since the intrinsic fluorescence line shape and intensity were measured at multiple excitation wavelengths with high accuracy, we were able to construct intrinsic fluorescence EEMs for the minced tissue. Figure 8 shows fluorescence EEMs obtained from (a) a thick sample of minced tissue, (b) a thin layer of minced tissue on a microscope slide (intrinsic fluorescence), and (d) the intrinsic fluorescence EEM of the sample in (a) extracted with Eq. (3). The similarity between the extracted intrinsic minced tissue fluorescence EEM and that of the thin minced tissue slide EEM demonstrates that we can accurately extract intrinsic tissue fluorescence EEMs for hemoglobin concentrations as high as at least 4.7 g/l (70 μM).

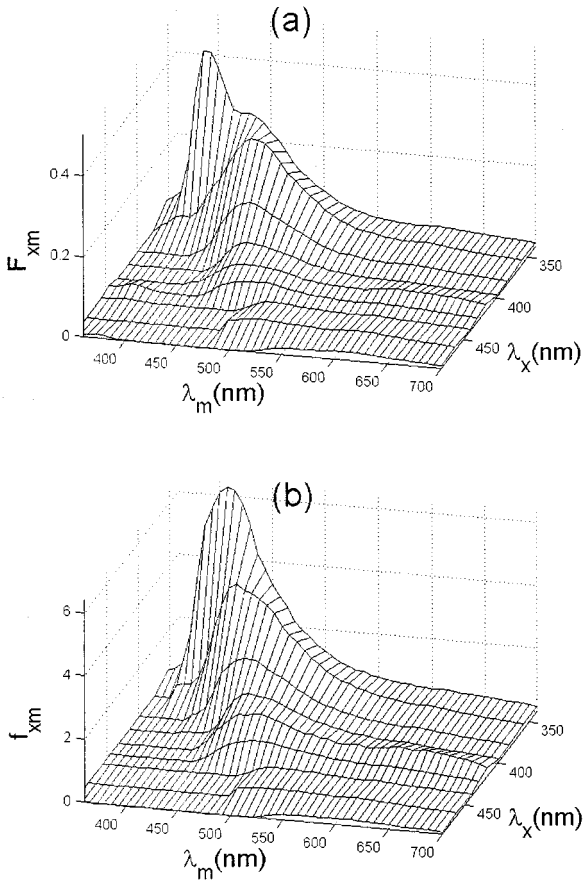

Fig. 9. Fluorescence EEMs of bulk oral cavity tissue *in vitro*. (a) bulk tissue (~5-mm thickness), (b) extracted intrinsic fluorescence. The similarity between (b) and Figs. 8(b) and 8(d) indicates that the influence of tissue layer structure on the intrinsic fluorescence is minor.

D. Bulk Tissue Studies

To explore the applicability of the method to bulk tissues, which generally have a layered structure, we studied the intrinsic fluorescence prior to and following mincing. We used normal buccal mucosa tissue of the oral cavity, which consists of a superficial layer of epithelium and underlying connective tissue. We found that, whereas the measured spectra acquired at different locations vary, the corresponding extracted intrinsic fluorescence line shapes were similar, suggesting that the differences are due to local variations in hemoglobin concentration. Furthermore, we found that the extracted intrinsic fluorescence line shapes of bulk tissue and its mince were quite similar [compare Figs. 9(b) and 8(d)]. This suggests that the layered architecture does not impair the ability of the photon migration method to extract the intrinsic fluorescence, at least for this type of tissue over the wavelength range of the experiments. We also studied the fluorescence of buccal mucosa *in vivo*, and found that the modeled intrinsic fluorescence spectra agreed with those obtained from *in vitro* tissues.

To summarize the results for the intrinsic fluorescence line shapes obtained through modeling and experiment, we compare in Fig. 10 extracted and measured intrinsic fluorescence spectra of minced tissue, extracted intrinsic fluorescence of bulk buccal mucosa tissue *in vitro* and *in vivo*, and measured minced tissue fluorescence, all excited at 337 nm. As can be seen, there are no significant differences between the various intrinsic fluorescence line shapes, suggesting that no major changes in normal oral mucosa tissue fluorophores occur in mincing tissue or when tissue biopsies are taken. We also applied the intrinsic fluorescence extraction method to spectra acquired *in vivo* from the esophageal mucosa of two patients, at 337-nm excitation (Fig. 11). Large variations in line shape and intensity of the measured fluorescence are clearly seen in Fig. 11(a). The intrinsic fluorescence, however, shows similar line shapes and intensities [Fig. 11(b)], supporting the hypothesis that the large fluorescence variations *in vivo* can be attributed to hemoglobin. Furthermore, these results demonstrate that the intrinsic fluorescence has to be used to extract biochemical information from clinically obtained fluorescence spectra.

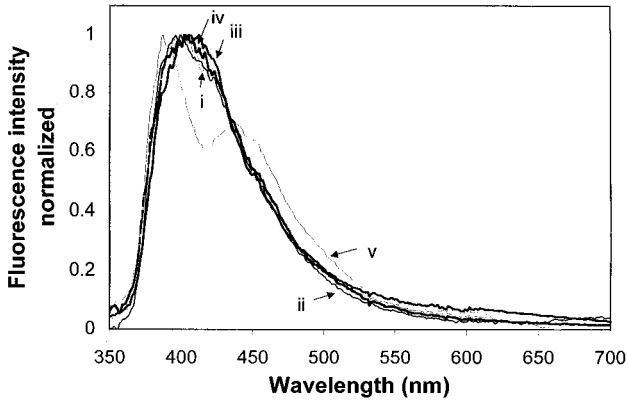

Fig. 10. Comparison of intrinsic fluorescence of bulk oral cavity tissue and minced tissue *in vivo* and *in vitro*. (i) Minced tissue, extracted intrinsic fluorescence; (ii) minced tissue, thin sample; (iii) bulk tissue *in vitro*, extracted intrinsic fluorescence; (iv) bulk tissue *in vivo*, extracted intrinsic fluorescence; (v) measured mince fluorescence, (uncorrected). All spectra are normalized. The intrinsic fluorescence spectra essentially collapse to the same line shape. However, the mince fluorescence shows major differences, mostly owing to distortions from hemoglobin absorption.

The intrinsic fluorescence EEMs can be decomposed into EEMs of constituent fluorophores to provide information about the biochemical composition of the tissue. We attempted to do this using EEMs of several types of collagen, elastin, and NADH (the major oral-tissue fluorophores in the near-UV–visible range), obtained from pure biochemicals in PBS (phosphate buffered solution) suspensions and solutions. In the case of normal buccal mucosa tissue the intrinsic fluorescence EEM could be fit in a variety of ways either with or without NADH. However, for the intrinsic fluorescence of cancerous tissue, which exhibits a significant redshift (peaking approx-

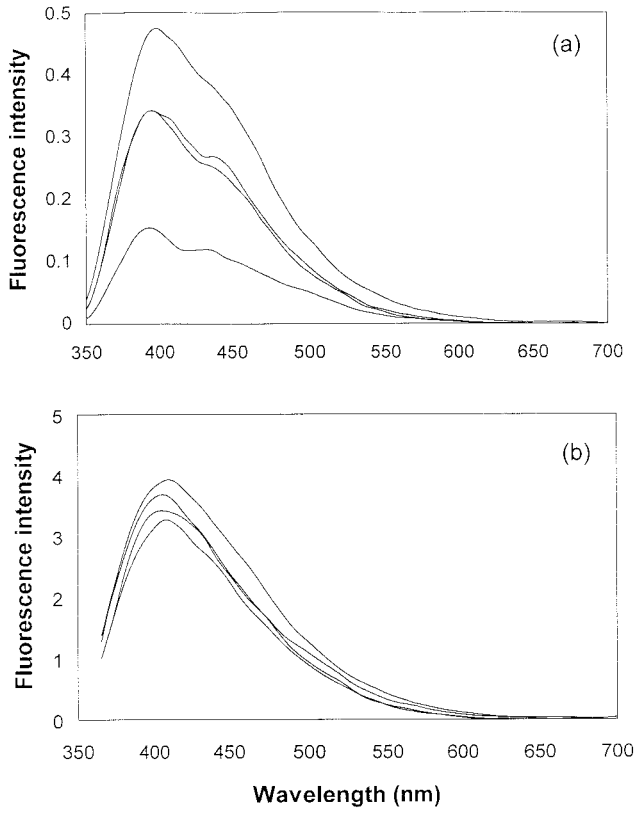

Fig. 11. *In vivo* fluorescence spectra of esophageal tissue from two patients. (a) Measured fluorescence, (b) intrinsic fluorescence. Note the variations in line shape and intensity in (a) and the similarity in spectra after extraction of the intrinsic fluorescence (b).

imately at 445 nm versus 405 nm for normal tissue with 337-nm excitation, Fig. 12), the use of NADH was essential, and a unique combination of type I and type IV collagen and NADH was required for a good fit. This suggests that NADH is more prominent in cancerous tissue than in normal tissue, possibly as a result of an increase in epithelial thickness and/or higher metabolic activity of the cells. However, lack

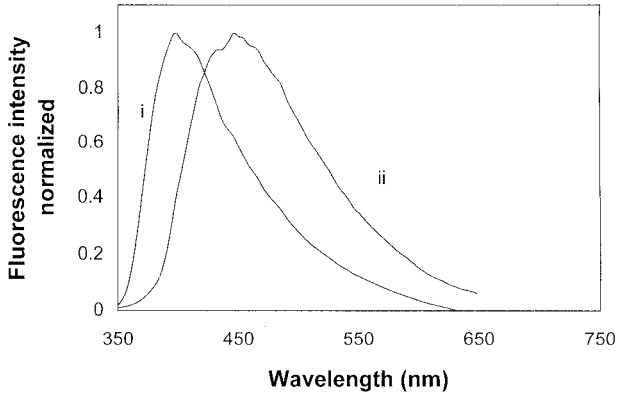

Fig. 12. *In vivo* fluorescence spectra from buccal mucosa tissue. Comparison of intrinsic fluorescence from a normal tissue site (i) and a cancerous site (ii). The large peak shift can be attributed to stronger NADH fluorescence.

of the uniqueness in the fits of normal tissue indicate that the use of chemically extracted fluorophores is not ideal, because of the broad spectral features and the spectral variations associated with different local environments and extraction methods. An alternative approach is under study in our laboratory.

5. Discussion

We have conducted studies to assess the distorting effects of scattering and absorption on fluorescence in turbid media, and the ability of our method to extract the undistorted intrinsic fluorescence from combined measurements of fluorescence and diffuse reflectance spectra. The method is based on the fact that the effects of scattering and absorption manifest themselves similarly in both diffuse reflectance and fluorescence. To examine the validity of the model, we studied physical tissue models, *ex vivo* tissue samples, and *in vivo* tissues. We considered the recovery of both fluorescence line shape and intensity for a wide range of physiologically relevant absorption and scattering coefficients.

As the excitation or emission light traverses the turbid medium it undergoes scattering and absorption. In the case of fluorescence the light undergoes a change to longer wavelength at some point (node) along its path. Spectral variations in scattering and absorption, the size of the probe, and other factors can alter the amount of light collected by the probe and give rise to line shape and intensity distortions.

We first discuss the effects of scattering in the *absence* of absorption. Scattering can affect the reflectance line shape, because our finite-size optical probe collects only a portion of the diffusely reflected light. This becomes important, because different spectral components scatter differently. Blue light usually has a shorter transport mean free path than red light.[19,40] Thus, it is localized closer to the probe, and more of it can be collected, distorting the reflectance line shape. The reflectance intensity increases approximately linearly with scatter concentration [Fig. 2(b)].

As expected from Eq. (4) and Monte Carlo simulations (Fig. 4), the dependence of the fluorescence line shape on scattering is much weaker than that of reflectance over the same wavelength range [Figs. 2(b) and 3(b)]. This difference is due to the fact that the emission portion of the fluorescence path is shorter than the reflectance path at that same wavelength (λ_m). The most important contribution to this pathlength reduction stems from the fact that fluorescence is a two-stage process, in which an excitation photon is converted to an emission photon at a longer wavelength. Thus fluorescence emission has to travel only approximately half the length of a reflectance photon path before it is collected by the probe. In addition, the wavelength change when a fluorescence photon is created gives rise to a change in scattering. These changes are built into the model through the wavelength dependence of μ_{sm}, μ_{sx}, g_x, and g_m. Finally, the isotropic nature of the fluorescence event allows fluorescence emission to return to

the tissue surface more readily than diffuse reflectance. However, this is less important when the fluorophores have a small absorption coefficient and quantum yield, because the excitation light tends to become randomized ($\mu_s' \gg \mu_{fx}$) before a fluorescence event occurs.

The variations in fluorescence intensity as a function of scattering are much more apparent than the corresponding line shape differences (Fig. 5). The fluorescence intensity depends on the mean free path of both excitation and emission light. In the weakly scattering regime (scatterer concentration <0.065 in volume percent, transport mean free path $1/\mu_s' > 4$ mm), the mean free path is long, and light can penetrate deep into the medium. There, fluorescence light is emitted isotropically, and only a portion can be collected by a probe of finite size. Even a small increase in scatterer concentration results in light being deflected off the probe collection angle by single (or possibly multiple) nondiffusive scattering events. Thus the intensity decreases rapidly. This behavior is not well described by Eq. (4), because the reflectance in Eq. (4) approaches zero in the absence of scattering. As the scattering concentration increases further (scatter concentration >0.065 in volume percent), the scattering becomes diffusive (the relevant range for biologic tissues). Both excitation and emission photons undergo increased scattering, have a smaller mean free path, and are more confined to the vicinity of the probe. This increases the probability of collection and leads to higher intensities, in agreement with Eq. (4).

When both absorption and scattering are present, the fluorescence line shape and intensity are distorted in a manner that is characteristic of the spectral features and concentrations of the absorber. Equation (3) describes these changes well, as demonstrated in experiments with physical tissue models and tissue samples (Figs. 6–11). We can understand the success of our model by examining the factors in Eq. (3). The absorption distortion of the intrinsic fluorescence emission line shape is mostly accounted for by the factor R_m/R_{0m}, which contains similar absorption information to that present in the measured fluorescence emission. The factor R_x/R_{0x} describes the attenuation of laser excitation light that is due to absorption and the concomitant reduction of the overall fluorescence intensity. Absorption affects fluorescence and reflectance differently because of their different photon path lengths. This difference is accounted for by the addition of the factor ϵ_m to the reflectance ratio in the denominator of Eq. (3); the higher its value, the smaller the importance of the factor R_m/R_{0m}.

The intrinsic fluorescence-correction factors of the photon migration method have to be obtained with physical tissue models. As explained above, the probe-specific parameter S was set equal to 1. The value of ϵ was $\sim$0.15 for the samples containing polystyrene beads and 0.05 for the minced tissue samples. These estimates were obtained with the value of S fixed, and Mie theory calculated values for g. The intensity scaling parameter, l, was approximately 220 μm. These values can vary with probe geometry, as discussed below. The parameters R_{0m}, R_{0x}, R_x, g, and μ_{sx} in Eq. (3), which are not directly measured from the experiment, can be extracted from the diffuse reflectance with a model suitable for our specific probe geometry.[19] For example, with the model of Zonios *et al.*[19] we can obtain the reduced scattering and absorption coefficient and thus determine these parameters.

The applicability of the model was also explored with *ex vivo* and *in vivo* tissues. We found that in the case of normal buccal mucosa our model successfully recovers the intrinsic fluorescence. Specifically, the intrinsic fluorescence of minced oral tissue, which consists of a homogenous mix of tissue fluorophores, is similar to that of intact oral tissue, which consists of two distinct relevant layers with different biochemical composition. This agreement can be explained by the fact that the top tissue layer (epithelium) is only weakly absorbing, scattering, and fluorescing in normal tissue. Thus, light penetration and distribution in the tissue is not affected significantly. Moreover, the epithelial layer is thin (50–300 μm) compared with the relatively large probe diameter (1.5 mm, N.A. = 0.22). As a result, the probe sampling depth is several times larger than the epithelial thickness, and we collect light traversing multiple photon paths (total transport mean free path in the medium, $1/\mu_t' \approx 0.3$ mm). However, for thicker epithelium or a smaller-diameter probe, this homogenous model may no longer be appropriate, since less connective tissue is sampled.

In our experiments, hemoglobin was the dominant absorber. However, the model is valid for turbid media consisting of any absorber. For example, experiments in arterial tissue indicate that the model recovers the intrinsic fluorescence accurately in the presence of the absorber beta-carotene.[41] Nevertheless, for extremely high absorption ($\mu_a > 3\mu_s'$) the assumptions that the fluorescence and reflectance have similar photon paths and that the phase function can be separated from scattering and absorption break down. As a result, the line shape and intensity of the intrinsic fluorescence cannot be extracted accurately, and distortions due to absorption are still observable.

The model assumes that tissue fluorophores do not contribute appreciably to the scattering-absorption behavior of the tissue. This is generally true for biologic tissue in the near-UV and visible range, where the fluorescence quantum yield and absorption are low and the absorption and emission bands do not significantly overlap. However, the model is not valid for fluorophores with high quantum efficiency and strong absorption. In this case the isotropic nature of the fluorescence is no longer negligible, because a fluorescence event can take place long before the excitation light is randomized, significantly shortening the resulting photon path. An example is Rhodamine dye, which has a high quantum yield, and overlapping absorption and emission bands. As

a result, Rhodamine fluorescence can also be observed in the reflectance spectrum. Additionally, reabsorption and reemission events can also take place, which are not accounted for by the method. Similarly, the intrinsic fluorescence of exogenous dyes, and endogenous fluorophores, such as tryptophan, an amino acid with high quantum yield, excited at shorter UV wavelength might not be well described by the method. In addition, tryptophan is mostly present in the epithelial layer, and that might invalidate the method's assumption of a homogenous medium.

Other researchers have used reflectance to correct distortions in fluorescence. A previous study used a simple division to recover the fluorescence line shape but not the intensity.[42] Mayevsky and Chance[23] and Renault *et al.*[43] conducted experiments with brain tissue and isolated perfused hearts, respectively. By measuring the NADH fluorescence of heart tissue while flushing the heart with oxygenated and nonoxygenated buffer and blood, they observed a decrease in fluorescence that is due to oxyhemoglobin and deoxyhemoglobin. To correct for this effect, they measured the fluorescence and the reflectance (as a reference) at different isosbestic wavelengths of hemoglobin. Renault *et al.*[43] assumed a simple exponential decrease with blood content, c, for fluorescence, $F = F_0 \exp(-k_1 c)$, and for reflectance, $R = R_0 \exp(-k_2 c)$. As a result, an expression was obtained, $F_0 = F/(R/R_0)^k$ with $k = k_1/k_2$ slightly larger than 1. F_0 denotes the fluorescence without blood absorption and is related to our parameter, f_{xm}, and k_1 and k_2 are experimentally measured constants. Renault's expression can be approximated by $F_0 = F/(R_m/R_{0m} + \epsilon)$, which reconstructs the emission part of Eq. (3), as described by the final factor in the denominator. However, Renault *et al.*[42] used this formula only for the absorption correction at one wavelength and did not take into account the absorption of the excitation light.

In summary, we have conducted experiments with physical tissue models, *ex vivo* tissue samples, and *in vivo* tissues to validate the ability of the photon migration method to extract the intrinsic fluorescence over a wide wavelength range of absorber and scatterer concentrations for excitation and emission wavelengths between 337 and 700 nm. We showed that the method can remove line shape and intensity distortions and that the intrinsic fluorescence can be recovered, which provides more-reliable information about the biologic constituents of the tissue. Although the above studies were directed toward fluorescence, the conclusions should be equally valid for Raman scattering. In this case the fluorescence event is replaced with a Raman scattering event, which is also isotropic. Lack of overlap between excitation and Raman scattering wavelengths, and the small cross sections characteristic of Raman scattering, are optimal for the performance of the method and should enable accurate extraction of the intrinsic intensity of a Raman band in a turbid medium.

Appendix A: List of Symbols

The following symbols appear in this paper:

F	fluorescence
R	reflectance
R_0	reflectance when no absorber present
x	subscript for excitation wavelength
m	subscript for emission wavelength
ρ	escape probability
w	corresponding weight (survival fraction) of the injected photon
a	albedo
I_x	excitation intensity
ν_x	excitation frequency
ν_m	emission frequency
μ_a	absorption coefficient
μ_s	scattering coefficient
μ_s'	reduced scattering coefficient
σ_s	scattering cross section
l	constant for given light delivery–collection scheme
f	intrinsic fluorescence
μ_{f_x}	fluorophore absorption coefficient
S	constant for specific light delivery–collection geometry
g	anisotropy coefficient
ϵ	$=\exp(\beta)-1$
β	$=S(1-g)$

This research was carried out at the Massachusetts Institute of Technology Laser Biomedical Research Center and supported by National Institutes of Health (NIH) grants RR02594, CA53717, and CA72517. Irene Georgakoudi acknowledges NIH National Research Service Award F32-CA80345. We thank Tulio Valdez and Ramachandra Dasari for helpful discussions.

References and Notes

1. K. T. Schomacker, J. K. Frisoli, C. C. Compton, T. J. Flotte, J. M. Richter, N. S. Nishioka, and T. F. Deutsch, "Ultraviolet laser-induced fluorescence of colonic tissue basic biology and diagnostic potential," Lasers Surg. Med. **12,** 63–78 (1992).
2. C. H. Liu, B. B. Das, W. L. S. Glassman, G. C. Tang, K. M. Yoo, H. R. Zhu, D. L. Akins, S. S. Lubicz, J. Cleary, R. Prudente, E. Celmer, A. Caron, and R. R. Alfano, "Raman, fluorescence, and time-resolved light-scattering as optical diagnostic-techniques to separate diseased and normal biomedical media," J. Photochem. Photobiol. B **16**(2), 187–209 (1992).
3. L. I. Laifer, K. M. O'Brien, M. L. Stetz, G. R. Gindi, T. J. Garrand, and L. I. Deckelbaum, "Biochemical basis for the difference between normal and atherosclerotic arterial fluorescence," Circulation **80,** 1893–1901 (1989).
4. P. K. Gupta, S. K. Majumder, and A. Uppal, "Breast cancer diagnosis using nitrogen laser excited autofluorescence spectroscopy," Lasers Surg. Med. **21,** 417–422 (1997).
5. C.-T. Chen, H. K. Chiang, S.-N. Chow, C.-Y. Wang, Y.-S. Lee, J.-C. Tsai, and C.-P. Chiang, "Autofluorescence in normal and malignant human oral tissues and in DMBA-induced hamster buccal pouch carcinogenesis," J. Oral Pathol. Med. **27,** 470–474 (1998).
6. M. Anidjar, O. Cussenot, S. Avrillier, D. Ettori, M. J. Villette, J. Fiet, P. Teillac, and A. Le Duc, "Ultraviolet laser-induced

autofluorescence distinction between malignant and normal urothelial cells and tissues," J. Biomed. Opt. **1,** 335–341 (1996).
7. G. I. Zonios, R. M. Cothren, J. T. Arendt, J. Wu, J. VanDam, J. M. Crawford, R. Manoharan, and M. S. Feld, "Morphological model of human colon tissue fluorescence," IEEE Trans. Biomed. Eng. **43,** 113–122 (1996).
8. N. Ramanujam, M. F. Mitchell, A. Mahadevan, S. Warren, S. Thomsen, E. Silva, and R. Richards-Kortum, "*In vivo* diagnosis of cervical intraepithelial neoplasia using 337-nm-excited laser-induced fluorescence," Proc. Natl. Acad. Sci. USA **91,** 10193–10197 (1994).
9. R. Richards-Kortum and E. Sevick-Muraca, "Quantitative optical spectroscopy for tissue diagnosis," Ann. Rev. Phys. Chem. **47,** 555–606 (1996).
10. M. Keijzer, R. R. Richards-Kortum, S. L. Jacques, and M. S. Feld, "Fluorescence spectroscopy of turbid media—autofluorescence of the human aorta," Appl. Opt. **28,** 4286–4292 (1989).
11. M. Kriegmair, H. Stepp, P. Steinbach, W. Lumper, A. Ehsan, H. G. Stepp, K. Rick, R. Knuchel, R. Baumgartner, and A. Hofstetter, "Fluorescence cystoscopy following intravesical instillation of 5-Aminolevulinic acid—a new procedure with high sensitivity for detection of hardly visible urothelial neoplasias," Urologia Internationalis **55,** 190–196 (1995).
12. G. A. Wagnières, W. M. Star, and B. C. Wilson, "*In vivo* fluorescence spectroscopy and imaging for oncological applications," Photochem. Photobiol. **68,** 603–632 (1998).
13. A. E. Profio, D. R. Doiron, and J. Sarnaik, "Fluorometer for endoscopic diagnosis of tumors," Med. Phys. **11,** 516–520 (1984).
14. P. Lenz, "Endoscopic fluorescence detector," Rev. Sci. Instrum. **59,** 930–933 (1988).
15. T. J. Farrell, R. P. Hawkes, M. S. Patterson, and B. C. Wilson, "Modeling of photosensitizer fluorescence emission and photobleaching for photodynamic therapy dosimetry," Appl. Opt. **37,** 7168–7183 (1998).
16. A. J. L. Jongen and H. J. C. M. Sterenborg, "Mathematical description of photobleaching *in vivo* describing the influence of tissue optics on measured fluorescence signals," Phys. Med. Biol. **42,** 1701–1716 (1997).
17. J. R. Mourant, I. J. Bigio, J. Boyer, R. L. Conn, T. Johnson, and T. Shimada, "Spectroscopic diagnosis of bladder cancer elastic light scattering," Lasers Surg. Med. **17,** 350–357 (1995).
18. F. Koenig, R. Larne, H. Enquist, F. J. McGovern, K. T. Schomacker, N. Kollias, and T. F. Deutsch, "Spectroscopic measurement of diffuse reflectance for enhanced detection of bladder carcinoma," Urology **51,** 342–345 (1998).
19. G. Zonios, L. T. Perelman, V. Backman, R. Manoharan, M. Fitzmaurice, J. Van Dam, and M. S. Feld, "Diffuse reflectance spectroscopy of human adenomatous colon polyps *in vivo*," Appl. Opt. **38,** 6628–6637 (1999).
20. J. B. Fishkin, O. Coquoz, E. R. Anderson, M. Brenner, and B. J. Tromberg, "Frequency-domain photon migration measurements of normal and malignant tissue optical properties in a human subject," Appl. Opt. **36,** 10–20 (1997).
21. F. F. Jöbsis, M. O'Connor, A. Vitale, and H. Vreman, "Intracellular redox changes in functioning cerebral cortex. I. Metabolic effects of epileptiform activity," J. Neurophysiol. **34,** 735–749 (1971).
22. A. Mayevsky and B. Chance, "Repetitive patterns of metabolic changes during cortical spreading depression of the awake rat," Brain Res. **65,** 529–533 (1974).
23. A. Mayevsky and B. Chance, "Intracellular oxidation-reduction state measured *in situ* by a multichannel fiber-optic surface fluorometer," Science **217,** 537–540 (1982).
24. C. Ince, J. M. C. C. Coremans, and H. A. Bruining, "*In vivo* NADH fluorescence," in *Oxygen Transport to Tissue XIV*, W. Erdmann and D. F. Bruley, eds. (Plenum, New York, 1992).
25. J. Wu, M. S. Feld, and R. P. Rava, "Analytical model for extracting intrinsic fluorescence in turbid media," Appl. Opt. **32,** 3585–3595 (1993).
26. A. J. Durkin, S. Jaikumar, N. Ramanujam, and R. Richards-Kortum, "Relation between fluorescence-spectra of dilute and turbid samples," Appl. Opt. **33,** 414–423 (1994).
27. N. N. Zhadin and R. R. Alfano, "Correction of the internal absorption effect in fluorescence emission and excitation spectra from absorbing and highly scattering media: theory and experiment," J. Biomed. Opt. **3,** 171–186 (1998).
28. C. M. Gardner, S. L. Jacques, and A. J. Welch, "Fluorescence spectroscopy of tissue: recovery of intrinsic fluorescence from measured fluorescence," Appl. Opt. **35,** 1780–1792 (1996).
29. M. S. Patterson and B. W. Pogue, "Mathematical model for time-resolved and frequency-domain fluorescence spectroscopy in biological tissues," Appl. Opt. **33,** 1963–1974 (1994).
30. S. K. Majumder, P. K. Gupta, and A. Uppal, "Autofluorescence spectroscopy of tissues from human oral cavity for discriminating malignant from normal," Lasers Life Sci. **8,** 211–227 (1999).
31. Q. Zhang, M. G. Müller, J. Wu, and M. S. Feld, "Turbidity-free fluorescence spectroscopy of biological tissue," Opt. Lett. **25,** 1451–1453 (2000).
32. In the current version we do not need to consider the effective albedo, a_{eff}, introduced in Ref. 25, because the new form of the escape probability [Eq. 2(b)] takes into account differences in optical properties at the excitation and the emission wavelengths. Additionally, we find that the previously introduced effective anisotropy coefficient, g_{eff}, does not significantly affect the resulting intrinsic fluorescence spectrum.
33. R. A. Zangaro, L. Silveira, Jr, R. Manoharan, G. Zonios, I. Itzkan, R. R. Dasari, J. Van Dam, and M. S. Feld, "Rapid multiexcitation fluorescence spectroscopy system for *in vivo* tissue diagnosis," Appl. Opt. **35,** 5211–5219 (1996).
34. R. M. Cothren, G. B. Hayes, J. R. Kramer, B. A. Sacks, C. Kittrell, and M. S. Feld, "A multifiber catheter with an optical shield for laser angiosurgery," Lasers Life Sci. **1,** 1–12 (1986).
35. A. J. Durkin, S. Jaikumar, and R. Richards-Kortum, "Optically dilute, absorbing and turbid phantoms for fluorescence spectroscopy of homogenous and inhomogenous samples," Appl. Spectrosc. **47,** 2114–2121 (1993).
36. U. Brackmann, *Lambdachrome Laser Dyes* (Lambda Physik GmbH, Goettingen, Germany, 1997).
37. O. W. van Assendelft, *Spectrophotometry of Haemoglobin Derivatives* (Thomas, Springfield, Ill., 1970).
38. H. C. van de Hulst, *Light Scattering by Small Particles* (Dover, New York, 1957).
39. G. I. Zonios, "Diffuse reflectance spectroscopy of human colon tissue," Ph.D. dissertation (MIT, Cambridge, Mass., 1998).
40. J. R. Mourant, J. P. Freyer, A. H. Hielscher, A. A. Eick, D. Shen, and T. M. Johnson, "Mechanisms of light scattering from biological cells relevant to noninvasive optical-tissue diagnostics," Appl. Opt. **37,** 3586–3593 (1998).
41. S. W. E. van de Poll, M. G. Müller, Q. Zhang, J. Myles, J. R. Kramer, and M. S. Feld, "Combined fluorescence and reflectance spectroscopy of arterial wall improves the identification of atherosclerosis," Circulation **100,** 2349, Suppl. S Nov. 2 (1999).
42. H. Zeng, C. MacAulay, D. I. McLean, and B. Palcic, "Spectroscopic and microscopic characteristics of human skin autofluorescence emission," Photochem. Photobiol. **61,** 639–645 (1995).
43. G. Renault, E. Raynal, M. Sinet, M. Muffat-Joly, J.-P. Berthier, J. Cornillault, B. Godard, and J.-J. Pocidalo, "*In situ* double-beam NADH laser fluorimetry: a choice of a reference wavelength," Am. J. Physiol. **246,** H491–H499 (1984).